

# Emission Factors and Real-Time Optical Properties of Particles Emitted from Traditional Wood Burning Cookstoves

CHRISTOPH A. RODEN\* AND  
TAMI C. BOND

*Department of Civil and Environmental Engineering,  
University of Illinois at Urbana-Champaign,  
205 North Mathews Avenue, Urbana, Illinois 61801*

STUART CONWAY

*Trees Water & People, 633 Remington Street,  
Fort Collins, Colorado 80524*

ANIBAL BENJAMIN OSORTO PINEL

*AHDESA, Colonia Country Club, Calle Principal Casa No  
2245, Comayagua, MDC Honduras*

It is estimated that the combustion of biofuel generates 20% of all carbonaceous aerosols, yet these particles are studied less than those of other common sources. We designed and built a portable battery-operated emission-sampling cart to measure the real-time optical properties and other emission characteristics of biofuel cookstoves. In a field study in Honduras, we measured emission factors averaging 8.5 g/kg, higher than those found in previous laboratory studies. Strong flaming events emitted very dark particles with the optical properties of black particles. The elemental carbon to total carbon ratios ranged from 0.07 to 0.64, confirming that high elemental carbon fractions can be emitted from biofuel combustion and may not be used to distinguish fossil-fuel from biofuel sources when cooking is the dominant usage. Absorption Ångström exponents, representing the dependence of absorption on wavelength, ranged from 1 (black) to 5 (yellow). Strongly absorbing particles with absorption inversely dependent on wavelength were emitted separately from particles with weak absorption and strong wavelength dependence; the latter probably contained conjugated aromatic compounds. Because combustion occurs in distinct phases, different types of carbonaceous aerosols from biofuel combustion are externally mixed at emission and may have different atmospheric fates.

## Introduction

More than two billion people use biofuels such as wood, crop residue, and dung as their primary energy source for domestic needs such as heating and cooking (1). Biofuel is responsible for a significant fraction of global black carbon (BC) and organic carbon (OC) aerosol. It is estimated to contribute 20% of primary pyrogenic BC and OC globally and 33 and 65%, respectively, of energy-related pyrogenic BC and OC (2). Although these values are similar to the

estimated contribution of diesel engines, 37 and 16% of energy-related BC and OC, biofuel sources have been far less studied than vehicular emissions.

BC and OC are important contributors to the Earth's radiative balance; estimates of climate forcing range from 0.27 to 0.54 and  $-0.04$  to  $-0.41$  W/m<sup>2</sup>, respectively (3), compared with a CO<sub>2</sub> forcing of 1.45 W/m<sup>2</sup>. In addition to emitted quantities, the chemical composition and optical properties of emissions must be known for climate modeling. Most of the particles from biofuel combustion are carbonaceous (4), and the difference between BC and OC is important. Black carbon absorbs radiation, warming the atmosphere and cooling the ground, while organic carbon primarily scatters light, cooling both the ground and atmosphere.

Some of the information needed for climate research is also of interest for urban and regional air quality studies. Chemical composition is needed for source apportionment studies, in which the elemental carbon fraction may be used as a tracer for vehicle exhaust (5). Particle mixing, or the coexistence of two substances in a single particle, may affect the rate of particle removal from the atmosphere; BC may have a longer atmospheric lifetime than OC (6). Black carbon from combustion affects pollutant partitioning, particularly for polyaromatic hydrocarbons (7). If BC is coated by material at emission, its surface may not be available to adsorb gaseous or aqueous pollutants.

Several studies have measured biofuel combustion emissions (8–12). However, these early studies provide insufficient information for several reasons. First, it is not known if the laboratory experiments are similar to everyday cooking practices. Whereas laboratory experiments strive for uniformity and repeatability, emissions depend on fuel type, heat required by different food types, and the cook's skill and attention level. Field studies have reported gas-phase pollutants (13, 14), but not particulate matter, except for one study which measured simulated cooking (15). Second, particulate chemical composition has only recently been reported in one laboratory study (16). Climate-relevant properties such as absorption and scattering have been examined only for other dissimilar sources, such as open biomass burning (17). Finally, none of the studies have reported real-time data. As we will show, such information can be valuable in inferring the nature of the particles.

Two limitations account for the minimal field data. First, it can be difficult to obtain access to real sources, and second, biofuel is often used in remote locations where lack of power restricts measurement capabilities. The present study overcomes both of these challenges. We designed and built a mobile emission measurement platform, the ambulatory real-time analyzer for climate and health-related noxious emissions (ARACHNE), which measures emission factors and real-time optical properties of emissions in remote locations. A long-standing collaboration between the University of Illinois, Trees Water and People (a U.S.-based nonprofit organization), and the Honduran Association for Development (AHDESA), a Honduran nonprofit organization, allowed us to access emissions from real cooking fires.

In addition to their climatic impacts, biofuel emissions also have other important adverse effects. High exposures from indoor combustion cause health problems such as acute respiratory illness. Those most affected are children, the elderly, and people with compromised immune systems (18). Indoor smoke is estimated to be the eighth-highest contributor to the global burden of disease (19). The optimal

\* Corresponding author e-mail: croden@uiuc.edu; phone: (217) 333-7773; alternate phone: (217) 333-6967; fax: (217) 333-6968.

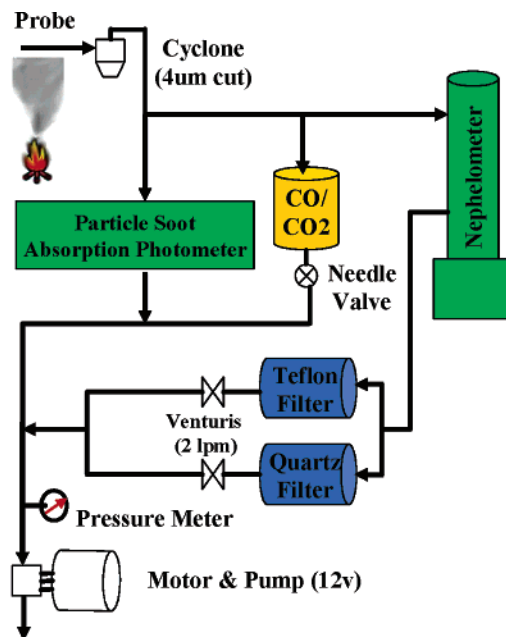
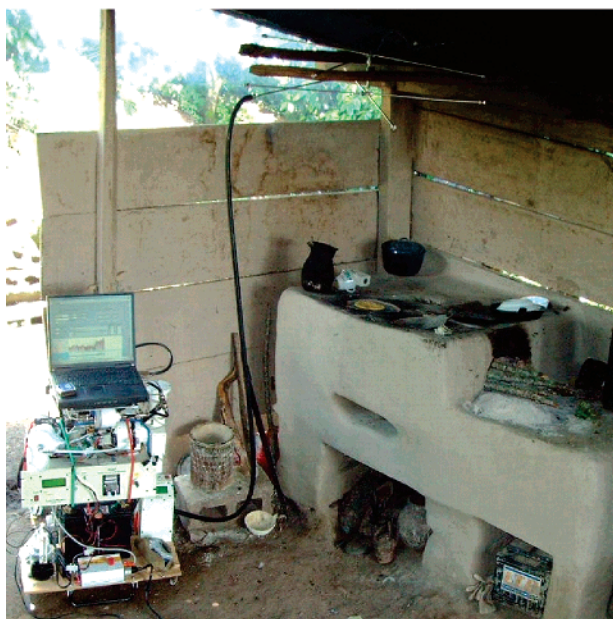


**FIGURE 1.** Photograph of sampling cart setup, including the probe, next to a traditional Honduran cookstove and a schematic of emission sampling cart.

goal of the partnership between our university and the nonprofit organizations was the development and dissemination of improved cookstoves to improve the health and livelihoods of Honduran people. The emission characterization described here has been a secondary benefit.

## Methods

Figure 1 contains a schematic and photograph of our portable sampling system, probe, and a traditional Honduran cookstove. The ARACHNE measures real-time absorption and scattering by particles, carbon monoxide (CO), and carbon dioxide (CO<sub>2</sub>) concentrations. It also collects particles on filters for chemical analysis. The system draws approximately 100 W and is powered by an automobile battery, which provides a run-time of about 5 h. The package sits in an aluminum frame attached to a luggage dolly and measures about 60 × 92 × 47 cm (*W* × *H* × *D*). The Supporting Information provides more details about system characterization.

Accepted methods of sampling particulate emissions include collecting the plume in an exhaust hood (20) and drawing a single sample after mixing the exhaust or traversing the exhaust with a single probe (21). Neither of these methods allows collection of a real-time, representative sample from an unsteady combustion source, while minimizing disturbance to the emission plume and the cooking. The dilution rate (22) and dilution ratio (23) affect the sample, so that many sampling approaches use either a large dilution plenum (24) or a dilution tunnel (22). Neither of these was practical in this study. We sampled the plume with an eight-armed stainless-steel probe, 1 m in diameter, which covered most of the emission plume. The probe was suspended 1–1.5 m above the cookstove, so the initial 1–1.5 s of dilution and entrainment of ambient air occurred naturally. The Supporting Information contains further details, including the effect of nonisokinetic sampling, estimated at 1% loss of particle mass. We used the carbon balance method, detailed later, to determine emission factors (10, 23), so placement of the probe was not critical. For this method, it is more important that the collected sample contains a representative fraction of particulate and gaseous emissions, which we accomplished by sampling at 24 points centered in equal areas. Dilution is also used to reduce moisture in the sampled

exhaust, especially to prevent condensation. In this case, the exhaust is already dilute when sampled and ambient air is dry, with typical ambient relative humidity (RH) ranging from 36 to 62%, so condensation does not occur.

After the probe, the emission sample travels ~3 m through conductive tubing to the ARACHNE. Particle loss through this tubing is measured at about 2% (see Supporting Information). When the gas reaches the instruments, its temperature has cooled to a few degrees above ambient. A cyclone (URG, URG-2000-30EN) removes particles larger than 4 μm before the sample is divided. One branch enters a three-wavelength particle soot absorption photometer (Radiance Research, PSAP), which measures absorption at 467, 530, and 660 nm. A second flow is filtered before carbon dioxide and carbon monoxide are measured (CO<sub>2</sub> Telaire, 6004-S50K; CO City Technology, 3ME/F CiTiceL). The third flow passes through a single-wavelength nephelometer (Radiance Research, M903) which measures light scattering at 530 nm. The optical measurements were orders of magnitude above their detection limits, and the main challenge was keeping concentrations below the upper measurement limit. We calculated absorption from the raw PSAP filter transmission data and corrected it for spot size, flow rate, and light scattering (25). Compared with other filter-based methods for measuring absorption, the PSAP has the advantage of producing continuous real-time data, since the filters can be changed in about 15 s. While apparent filter-based absorption can be affected by sharp changes in RH (26), the magnitude of this effect appears to be less than 50 Mm<sup>-1</sup> for a 10% change in RH over a few minutes. Our maximum RH was about 6% above ambient (see Supporting Information), so fluctuations would be lower; uncertainties would affect a typical signal by less than 1%. System RH does affect the scattering signal, and this potential effect will be discussed later.

Two filters with equal flows collect particles downstream of the nephelometer; this location minimizes total system flow and conserves power. The measured particle loss through the nephelometer was approximately 2% (see Supporting Information). All flows are drawn through the system with a vacuum pump (Cole Parmer, A-79200-40). Real-time instrument data is collected on a laptop.

**TABLE 1. Summary of Honduras Field Tests**

test	pressure (mbar)	temp (K)	RH (%)	length (min)	stove type	chimney condition	EF obtained	notes; food cooked
1	887	302	51	120	traditional	none	yes	noodles, tea
2	887	302	50	120	traditional	none	no	no actual cooking
3	891	303	50	120	traditional	clogged	yes	tortillas
4	889	301	50	120	traditional	none	yes	left-overs, coffee
5	885	300	54	240	traditional	none	yes	large pot of beans
6	885	300	57	120	traditional	clogged	yes	reheated rice and beans
7	886	303	51	200	improved	functional	yes	beans, rice, eggs
8	888	299	47	155	traditional	none	yes	tortillas
9	889	297	62	240	traditional	open	yes	coffee, boiling beans
10	889	302	50	165	same as 9	open	no	did not cook, fire smoldered out
11	893	305	44	175	traditional	none	yes	pasta, chicken
12	890	306	36	120	traditional	none	yes	tortillas
13	888	303	49	100	traditional	clogged	yes	reheated beans
14	892	301	62	145	traditional	open	yes	boiling beans
15	881	302	57	120	improved	functional	no	exhaust not captured

Flows through the filters are controlled with critical flow venturis (27). Provided with an upstream pressure of one atmosphere and a minimum pressure drop of 270 mbar, these venturis maintain a constant 2 L/min flow, even if battery power and downstream pressure decrease. The gradual filter loading does introduce a slight upstream pressure change, but the maximum filter loading was 160 ug/cm<sup>2</sup> resulting in a pressure change of less than 1%. The flows were calibrated in Honduras with a bubble meter and adjusted to standard temperature and pressure.

We used PFTE membrane filters (Millipore Fluoropore, 1 um pore size) to determine PM mass and quartz-fiber filters (Pall QAT-UP) to measure organic and elemental carbon. To account for positive adsorption artifacts, we placed a quartz backup filter behind the Teflon filter, in addition to the separate primary quartz filter (4, 28). The PFTE filter masses were determined with a Cahn C-31 microbalance. Prior to the weight measurement, the filters were equilibrated in a temperature and humidity controlled room (25 °C, 50% relative humidity) for 24 h and charge neutralized immediately before weighing with a Po<sup>210</sup> source. Both PTFE and quartz field blanks were collected and subtracted from the measured samples. The quartz filters were baked before sampling at 550 °C, stored individually in sealed containers lined with baked aluminum foil, and kept in a freezer. The quartz filters were analyzed for organic carbon (OC) and elemental carbon (EC) with a Sunset Laboratory carbon analyzer, commonly termed “NIOSH Method 5040”. The measured concentrations from the backup quartz filters were subtracted from those of the primary quartz filters, and the difference was treated as the mass of particulate carbon for all subsequent calculations, including emission factors. Temperature profiles for this analysis are those recommended by the manufacturer and are given in Supporting Information.

We measured Honduran wood-fired cookstove emissions during the summer of 2004, as summarized in Table 1. We focus on traditional cookstoves here; improved cookstoves were also measured, but not enough tests were available to characterize them. Traditional cookstoves in this region typically have a U-shaped cross-section when viewed from the top (see photos in Supporting Information). Pots are placed directly on the fire or metal plates covering the fire are used for cooking surfaces. Fuel wood, which measured ~70 cm long with a 6 × 6 cm cross-section, is added through the open front of the stove. Stoves were located in either outdoor covered patio areas, separate stand-alone structures, or interior kitchens. The areas were generally well ventilated, and the emissions dissipated quickly after cooking. Five traditional stoves had chimneys: all were poorly functioning or fully blocked. Exhaust escaped from all stove openings

including the fuel-loading opening, around the edges of the pot or cooking surface, and weakly through unblocked chimneys where present. The two improved stoves had small front openings and working chimneys, and we sampled at the chimney exhaust since the indoor plume was negligible.

Each test began about 30 min before the start of cooking. We measured background CO<sub>2</sub>, CO, absorption, and scattering before and after the cooking events. Averages of these background measurements were subtracted from the concentrations measured during cooking. CO<sub>2</sub> contribution from human respiration was estimated to be 0.5–6% of the total increase and is included in our error analysis. Absorption and scattering background averaged one to two percent of the values during cooking and were also subtracted. We also adjusted for this background contribution when calculating PM emission factors.

Cooking events varied from preparing full meals to reheating leftovers. The food included stews, rice, beans, and tortillas. There was no meat frying or deep frying, which could have been a significant additional source of organic carbon. Sampling times varied from 1.5 to 4 h, depending on the cooking task. We obtained wood samples from each test site and placed them in double Ziploc bags. These samples were later analyzed for wood moisture by weighing and then drying the wood at 105 °C. Wood moisture varied between 10 and 30%, averaging 17%.

Wood was generally bought locally or scavenged and was the bulk of the fuel. Occasionally, the homeowners threw small pieces of trash including plastic, scrap paper, and food wrappers into the fire. If no hot coals were present to start the fire, scrap paper, kindling, or “ocote” were used. Ocote is a resinous pine that ignites easily but produces sooty smoke. After cooking was completed, the fires were usually left to burn out. Small ends of unburned wood were often thrown into the fire, not saved for the next meal.

Emission factors were determined using the “carbon balance” method. The amount of carbon per kilogram of wood typically varies between 0.45 and 0.55, depending on the type of tree. The firewood used in our study consisted of primarily oak and pine species, which have an average carbon content of 0.50 kg of carbon/kg of fuel with a standard deviation of 0.02 (29). During combustion, most of the carbon becomes CO and CO<sub>2</sub>, and neglecting the other carbon species (methane, non-methane hydrocarbons, and carbonaceous aerosols) may introduce an error of 1–4% (9, 10). Therefore, emitted CO<sub>2</sub> and CO can serve as a proxy for the fuel combusted, when adjusted for the carbon fraction of the fuel and for the ambient background. The ratio between pollutant and carbon as CO and CO<sub>2</sub> is an approximate emission factor. The equation below is used to determine

PM emission factors: all terms are at standard temperature and pressure.

$$EF\left(\frac{\text{g}_{\text{PM}}}{\text{kg}_{\text{wood}}}\right) = \left(\frac{\text{filter}_{\text{mass}}}{\text{volume}_{\text{sampled}}}\right) \times \left(\frac{1}{\Delta_{\text{CO}_2} + \Delta_{\text{CO}}}\right) \times \left(\frac{\text{m}^3_{\text{CO}_2}}{0.4905 \text{ kg}_C}\right) \times \left(\frac{0.5 \text{ kg}_C}{\text{kg}_{\text{wood}}}\right) \quad (1)$$

Since the CO and CO<sub>2</sub> measurements are critical for the carbon balance method, we paid particular attention to these sensors, comparing their responses to more accurate laboratory instruments. We performed multipoint calibrations of the sensors at typical field concentrations to determine repeatability and span accuracy and incorporated these factors into the error analysis.

**Intensive Optical Properties.** Two properties that can be determined from absorption and scattering are the single scatter albedo (SSA) and the absorption Ångström exponent ( $\dot{A}_{\text{ap}}$ ). In this study, we use real-time measurements of both SSA and  $\dot{A}_{\text{ap}}$  to determine the type of particles emitted from each phase of combustion.

SSA is defined as scattering divided by scattering plus absorption. It has been used as a measure of climatic impact; values below about 0.85 are thought to be climate warming (30). Flame-generated absorbing carbon has an SSA value of about 0.15–0.3. Such low values of SSA imply that very little nonabsorbing material is present.

$\dot{A}_{\text{ap}}$  is a measure of how the absorption by particles ( $B_{\text{ap}}$ ) depends on wavelength of the incident radiation ( $\lambda$ ), and is defined as

$$\frac{B_{\text{ap}}(\lambda_1)}{B_{\text{ap}}(\lambda_2)} = \left(\frac{\lambda_1}{\lambda_2}\right)^{-\dot{A}_{\text{ap}}}$$

For absorbing particles of constant imaginary refractive index that are small relative to the wavelength of light,  $\dot{A}_{\text{ap}}$  is 1.0 (31). Higher values suggest a spectrally dependent imaginary refractive index, which can be attributed to compounds with conjugated aromatic rings (32). PSAP measurements are unaffected by gaseous absorption and can be used to determine  $\dot{A}_{\text{ap}}$ .

## Results and Discussion

**Real-Time Measurements.** Cooking fires exhibited three general combustion phases, which we named vigorous flaming, gentle flaming, and smoldering. Figure 2 illustrates these phases using real-time data from test 5. Figure 2a and b demonstrates the beginning of vigorous flaming and the transition into the gentle flaming phase. Vigorous flaming is characterized by strong flames with a jutting appearance, resulting from rapid devolatilization from the wood. It occurs shortly after the ignition of added wood. During this phase, the emissions of particles are very high, especially dark, light-absorbing particles associated with low instantaneous single-scatter albedos. These events appear in Figure 2a as large increases in absorption and smaller increases in scattering, with a slower increase in CO<sub>2</sub> emissions. The first event in Figure 2a is preceded by a short scattering peak, when release and subsequent condensation of volatile matter occurs before the gases burst into flame. The second peak in Figure 2a shows immediate ignition, where large absorption and smaller scattering occur immediately after fuel addition. CO<sub>2</sub> usually peaks toward the end of vigorous flaming. This phase generally lasts between 1 and 5 min before the fire enters what we named the gentle flaming phase.

Gentle flaming is characterized by smaller flames, lower emission of scattering and absorbing particles, and a gradual decrease in CO<sub>2</sub>. Scattering and absorption coefficients were often similar in magnitude during this phase, indicating that

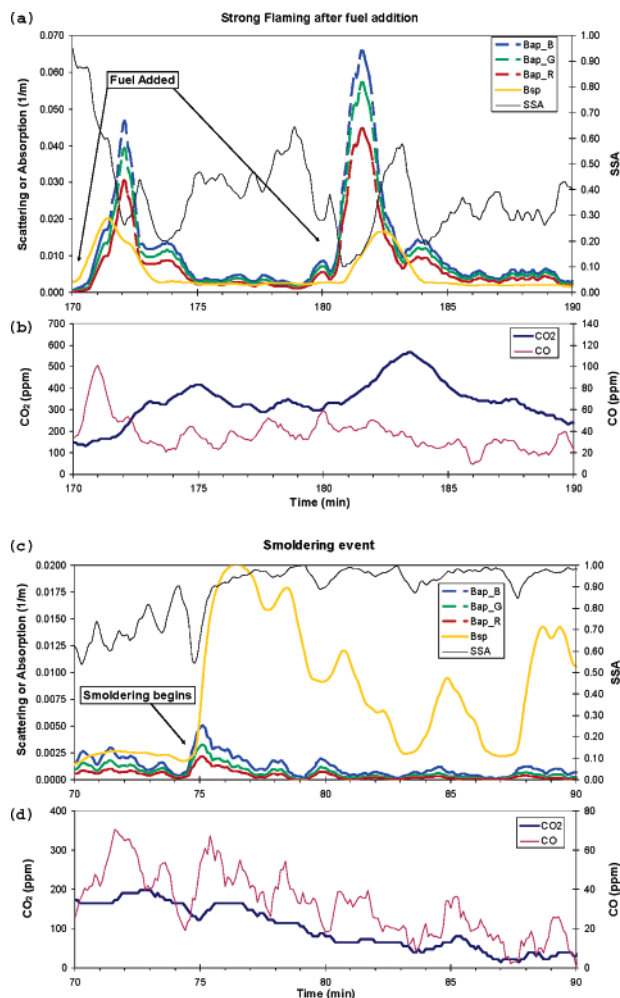


**FIGURE 2.** Real-time measurement results from test 5. Flaming conditions are shown in a and b; smoldering conditions are given in c and d. All values are shown as 40 s moving averages. Graphs a and c show scattering and absorption vs time. Scattering is the heavy yellow solid line. The absorption values at three different wavelengths (blue, green, and red) are shown as broken blue, green, and red lines, respectively. SSA is the thin black line. Graphs b and d are the CO and CO<sub>2</sub> concentration (CO is the thin purple line with units on the right axis; CO<sub>2</sub> is the thick dark blue line with units on the left axis).

both strongly absorbing and nonabsorbing particles were emitted. Carbon monoxide concentration followed either the scattering or absorption coefficient, but there was no consistency between tests. A small scattering peak might be observed simultaneously with a very large CO peak or vice versa.

The last phase, smoldering, occurs when the flames have extinguished. Figure 2c and d shows real-time data from such an event during test 5; note that the extinction scale is smaller than that for the flaming data. Light scattering increases sharply because flames are not consuming the volatile matter emitted from the wood, which recondenses into particles. Despite the lack of flame to create black carbon, these aerosols still have an absorbing component: SSA is generally between 0.9 and 1.0. Carbon monoxide emissions increase slightly at the beginning of this event, but quickly taper off. Although CO emissions are often associated with smoldering (33), the CO emissions here are no greater than those of the preceding gentle flaming phase. The decreasing carbon dioxide concentration shows a drop in burning rate.

Figure 3 shows the real-time absorption Ångström exponent during the last 90 min of a cooking cycle. During

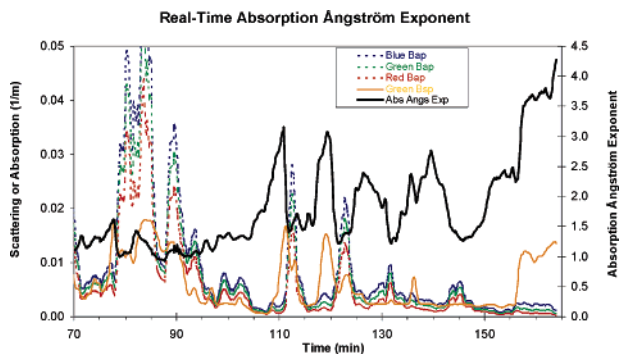


**FIGURE 3.** Real-time absorption characteristics measured during test 8.  $\hat{A}_{ap}$  absorption, and scattering vs time. (The absorption Ångström exponent is the thick solid black line with units on the right axis. Scattering is the thin yellow solid line. Blue  $B_{ap}$  is the broken blue line; green  $B_{ap}$  is the broken green line, and red  $B_{ap}$  is the broken red line. All absorption and scattering units are shown on the left axis.)

the vigorous and gentle flaming phases,  $\hat{A}_{ap}$  averages around 1.3, close to the black-particle value of 1.0. For individual tests, the average ranges between 0.9 and 1.9. These values are associated with low SSA; emissions from flaming conditions have the characteristics of black particles. Once the fire enters the smoldering phase, the absorption Ångström exponent continually increases toward values between 3.5 and 6. These may be thought of as particles containing PAH or other constituents that absorb strongly at UV wavelengths. After smoldering begins,  $\hat{A}_{ap}$  increases either until new fuel is added and flaming combustion is reinitiated or until smoldering ends.

The  $\hat{A}_{ap}$  values observed here are higher than those observed for mixed aerosol from solid-fuel combustion (32, 34). Figure 3 shows that  $\hat{A}_{ap}$  varies during a single fire and that high values are associated with weakly absorbing particles (SSA between 0.9 and 1). The distinct combustion phases, separated in time, suggest that highly absorbing particles with SSAs similar to pure EC are emitted at different times, therefore occurring in separate particles, than weakly absorbing material. This condition is known as external mixing.

Scanning electron microscope measurements have shown that individual particles with the shapes of black particles exist separately in open vegetative burning (35). However, such data characterize only a small fraction of the emitted particles. The extent of external mixing from biofuel stoves is further illustrated by Figure 4. This frequency plot is weighted by light extinction or absorption plus scattering. The  $x$  and  $y$  axes represent SSA and  $\hat{A}_{ap}$ , respectively, and are divided into 20 bins each. Each 6 s time period from all traditional stove tests is classified into one of the 400 bins. The plot includes only data from traditional stoves, with each test weighted equally.

Black particles (low SSA between 0.2 and 0.4, absorption Ångström exponent near 1.0) contribute most to the extinction. If nonblack compounds are present in the particulate matter, the single-scattering albedo should increase. Only a small fraction of these dark particles have SSA values higher than about 0.4. Particles with SSA around 0.9 and  $\hat{A}_{ap}$  between 3.0 and 4.5 are the second largest contributor to extinction. These particles probably contain organic material with conjugated aromatic rings and are generally associated with smoldering. For biofuel combustion, which occurs in distinct phases, these two classes of particles are emitted separately; only a small fraction of the data lies between these peaks. Because particles with different characteristics are emitted separately, they may have different rates of reaction in the atmosphere and different removal rates. For example, soluble

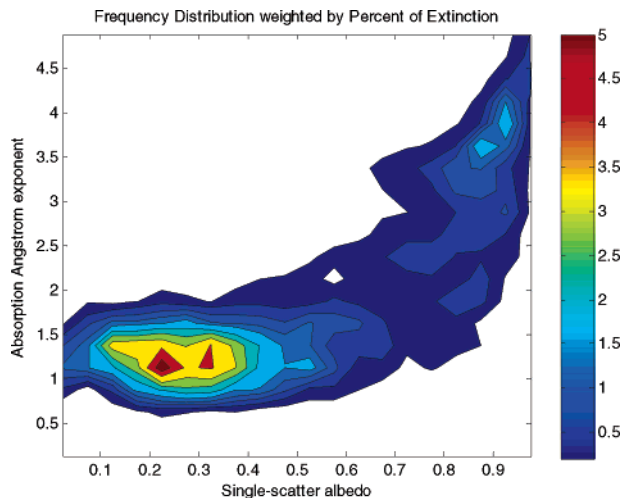


**FIGURE 4.** Frequency plot of the optical properties of emissions from traditional stoves. Every real-time data point (6 second time slice) is categorized into one of 400 bins and weighted by extinction. Tests 2 and 10 were excluded because no cooking occurred.

components may favor removal by wet deposition, but most of the black particles are not emitted with potentially soluble organic compounds.

While aerosols from mobile or industrial sources may occur in internal mixtures (36), this assumption is not true when the combustion is composed of distinct phases. For sources that are mainly externally mixed, we suggest that an external-mixing profile based on sequential combustion conditions is more appropriate.

**Emission Factors.** We determined PM mass emission factors (EF) for 12 tests, using the mass of the PTFE filters. These are summarized in Table 2. Mass emission factors ranged from 4.9 to 16.1 g/kg of fuel, with an average and standard deviation ( $1 - \sigma$ ) of  $8.5 \pm 3.6$  g/kg. The average uncertainty for the tests is 19% of the emission factor. The single-emission factor from an improved stove (test 7) was one of the lowest. Table 2 also includes EC and OC emission factors. The mass emission factor is not correlated with EC ( $R^2 = 0.0013$ ) but is highly correlated with OC ( $R^2 = 0.934$ ). The EC to total carbon (TC = EC + OC) ratio ranged from 0.07 to 0.64, with an average of 0.30, while the EC/PM ratio averaged 0.21.

The total mass associated with carbonaceous aerosols, defined as organic matter plus EC, is estimated from the EC and OC measurements. Organic matter (OM), or organic carbon plus associated elements, is usually estimated from OC measurements. Typical OM/OC ratios vary between 1.2 and 3.1 depending on the source and age of the aerosol (37). We use a value of 1.9 suggested for fireplace combustion of pine or oak (37). The estimated OM + EC emission factor usually agrees well with the PM emission factor. Other constituents could include ionic compounds and trace metals. These are generally less than 1% for wood smoke, but they could be as high as 20% for very hot combustion (4).

There was no correlation between wood moisture and PM emission factor or EC/TC fraction. Although moisture content is expected to affect emissions (18), we hypothesize that other factors, such as practice, cause greater variation in emissions, preventing us from seeing the effect of moisture content.

The uncertainty listed in the table for the OC and EC measurements is determined from that given by the Sunset analyzer. Temperature profile and co-collected trace constituents can greatly affect the elemental carbon versus organic carbon split (38, 39). Our estimated uncertainty does

**TABLE 2. Mass, OM + EC, OC, and EC Emission Factors, EC/TC Ratio, CO Emission Factors, Mass-Scattering Cross-Section, and Mass-Absorption Cross-Section for Twelve Tests<sup>a</sup>**

test	mass emission factor (g_PM/kg)	OM + EC emission factor (g/kg)	OC emission factor (g_OC/kg)	EC emission factor (g_EC/kg)	EC/TC	CO emission factor (g_CO/kg)	mass-scattering cross-section (m <sup>2</sup> /g)	mass-absorption cross-section (m <sup>2</sup> /g)
1	11.7 ± 1.9	10.7 ± 1.8	4.7 ± 0.9	1.7 ± 0.3	0.26 ± 0.02		2.1 ± 0.7	2.5 ± 0.5
3	6.5 ± 1.4	7.0 ± 1.2	1.9 ± 0.5	3.4 ± 0.8	0.64 ± 0.04		1.5 ± 0.4	5.2 ± 0.9
4	5.0 ± 0.9	4.6 ± 1.0	2.3 ± 0.5	0.2 ± 0.0	0.07 ± 0.01		1.4 ± 0.3	0.4 ± 0.1
5	9.4 ± 1.2	10.3 ± 1.7	5.0 ± 0.9	0.9 ± 0.1	0.15 ± 0.01	125 ± 41	1.8 ± 0.5	1.7 ± 0.3
6	16.1 ± 2.1	22.1 ± 4.8	10.5 ± 2.5	2.2 ± 0.5	0.18 ± 0.01	138 ± 30	2.2 ± 0.6	2.3 ± 0.4
7	5.6 ± 0.7	6.4 ± 0.7	1.7 ± 0.3	3.1 ± 0.5	0.64 ± 0.04	46 ± 19	1.6 ± 0.4	6.5 ± 1.1
8	10.3 ± 1.4	12.5 ± 1.9	5.2 ± 1.0	2.6 ± 0.5	0.34 ± 0.02	79 ± 32	2.2 ± 0.6	3.1 ± 0.6
9	4.9 ± 1.2	4.4 ± 0.9	1.4 ± 0.4	1.7 ± 0.5	0.55 ± 0.04	20 ± 46	2.2 ± 0.6	3.7 ± 0.7
11	5.3 ± 1.0	4.2 ± 0.9	2.0 ± 0.5	0.4 ± 0.1	0.16 ± 0.02	145 ± 55	2.2 ± 0.5	1.5 ± 0.3
12	5.7 ± 1.4	4.2 ± 0.8	1.6 ± 0.4	1.2 ± 0.3	0.43 ± 0.05	134 ± 63	1.6 ± 0.6	3.6 ± 0.9
13	9.9 ± 2.8	10.6 ± 3.0	5.4 ± 1.6	0.4 ± 0.1	0.07 ± 0.01	217 ± 97	3.3 ± 1.1	1.2 ± 0.3
14	11.7 ± 3.1	13.3 ± 3.5	6.7 ± 1.8	0.6 ± 0.2	0.08 ± 0.01	141 ± 108	2.8 ± 1.0	1.3 ± 0.3
av	8.5 ± 1.6	9.2 ± 1.9	4.0 ± 0.9	1.5 ± 0.3	0.30 ± 0.03	116 ± 55	2.2 ± 0.6	2.8 ± 0.5

<sup>a</sup> Uncertainties are 1σ.

not account for these factors; as with most source measurements, the values given here are operational definitions.

Table 2 also summarizes the CO emission factors, which range from 20 to 217 g/kg. (The CO sensor was not functioning during the first few tests.) Our average emission factor of 116 g/kg is slightly higher than previous cookstove studies by Zhang et al. (9) and Smith et al. (10), which averaged 69 and 100 g/kg, respectively. It is also comparable to previous measurements of fireplace emissions, which average 110–121 g/kg (40, 41).

The Teflon filter mass is used to determine the average scattering and absorption cross-section normalized to total particle mass, which are also listed in Table 2. The average mass scattering cross-section for all tests is 2.2 m<sup>2</sup>/g. The mass scattering cross-sections for submicron particles in ambient air are typically around 3 m<sup>2</sup>/g (42), but this value depends on particle size and chemical composition. Small absorbing particles scatter less than nonabsorbing particles of identical size and real refractive index; our data show that lower-mass scattering cross-sections correspond to higher-mass absorption cross-sections. As mentioned earlier, elevated values of relative humidity can increase the particle size and hence the scattering per unit of mass. This change is thought to be small, around 10% for organic material (43). The values of mass scattering efficiency in Table 2 are probably high bounds. However, changes in scattering because of RH dependence cannot affect SSA enough to change conclusions about the particle-mixing state, as shown in Figure 4.

**EC Fraction.** The EC to PM ratio, averaging 0.21, is much larger than that found for open vegetative burning (33) and for fireplaces (summarized by Bond et al., ref 2). Bond et al. (ref 2, section 5.6) discussed why EC ratios might vary, particularly between heating and cooking. Briefly, organic carbon is volatile matter emitted from heated wood, which can be consumed by passing through a flame. Carefully operated traditional stoves or open fires direct air flow toward the pot, so that air laden with volatile matter passes through the fire. Guiding the exhaust is less critical for heating applications, which rely on total heat release; only a small fraction of the wood energy is lost in unburned smoke.

Venkataraman et al. (16) reported EC/PM<sub>2.5</sub> mass fractions ranging from 0.05 to 0.52 for small cooking fires. Our results are very similar and provide independent confirmation that biofuel emissions can produce high EC fractions. Although the EC measurements are operationally defined, intercomparisons indicate that the EC values reported by our Sunset analyzer are often lower than those reported by other protocols (38), so the values reported here may be a lower

bound. This finding has implications for source apportionment. Novakov et al. (44) used an EC/TC ratio of 0.4–0.5 to estimate that about 80% of carbonaceous aerosol in the continental outflow from India came from fossil fuel combustion, but they used the EC/TC ratio from open vegetative burning. Other studies disagreed, using single-particle measurements to infer that biofuel contributed around 80% (45). Our results and those of Venkataraman et al. (16) indicate that EC/TC ratios in the Indian region may be closer to those of biofuel than previously thought. Values from open vegetative burning and fireplace burning should not be taken to represent cooking emissions.

**High PM Emission Factors.** Bond et al. (2) tabulate biofuel emission factors (see their Table 6), which we will only summarize here. Traditional cookstove emissions range from 1.0 to 2.8 g/kg, although one value of 6.4–8.9 g/kg, a second-hand citation from conference proceedings, suggests that higher values have been measured previously. Open cooking fires emit 0.9 to 5 g/kg, with the exception of 8.5 for eucalyptus chips. Our field emission factors of 4.9 to 16.1 are significantly larger than most of these values. They are closer to those of fireplaces, which average 5.1 to 10 g/kg (40, 41). Many factors such as size of fuel, wood moisture, timing of fuel addition, and stove design can influence PM emission factors from wood burning stoves (18, 40). These factors vary between stoves and usage conditions. We suggest two reasons for the difference between our field measurements and previous laboratory tests.

**Testing Procedure.** Laboratory tests often use a standard “water-boiling test” protocol (9–12). In this test, a given amount of water is brought to a boil and then simmered for a certain amount of time, usually 30 min. These tests often use uniform pieces of wood with similar moisture contents, and the wood is added at prescribed intervals. In the laboratory, exhaust flows are funneled through a hood for sampling, where exhaust flows in our field tests are essentially undisturbed.

**Ignition and High-Power Phase.** Accelerants used to start the fire, such as lighter fluid or paper (8, 9), are accounted for either by adding their mass to the fuel or by ignoring the first few minutes of emissions. However, these first few minutes often produce the most particulate matter, as Figure 2 attests. An important difference between lab-based tests and actual use is that lab-based tests may often only include one short “high-power” cooking phase of approximately 15 min. Honduran stoves operated in the high-emitting high-power or vigorous-flaming phase for a much greater fraction of the time. Either of these differences could cause the discrepancy between laboratory and field measurements.

**Outlook.** The significant difference from laboratory measurements implies that field measurements are needed as a reality check. Our study suggests that both emission factors and chemical composition are strongly affected by variables that differ between field and laboratory procedures. Although ARACHNE emission measurements may be less accurate than traditional source sampling, the ability to access real sources can identify biases that are much greater than the slightly reduced precision. The method also allows the use of real-time data to identify conditions associated with high emissions.

Although biofuel is an important regional and global source of particles, it will not be possible to measure emission quantities and properties for every region. To represent this source in global or regional emission inventories, the variables that control emission factors and environmentally relevant properties, such as EC/PM ratio and light absorption, need to be identified and quantified by region. These include wood type, size, and quality, local practices, and stove design; simply acquiring the appropriate fuel is insufficient. Measurements of emission quantities and properties should be linked with these variables and then used to produce regional emission estimates.

### Acknowledgments

We thank the many study participants who opened their homes to us and Augusto Ramirez and Wendy Naira who acted as our helpers and translators and are instrumental in the implementation of improved stoves. This project is supported by the National Science Foundation's Atmospheric Chemistry Program under Grant #ATM-0349292 and the U.S. Environmental Protection Agency's Partnership for Clean Indoor Air.

### Supporting Information Available

Additional graphics showing the sampling probe and examples of Honduran cookstoves and a further discussion of probe efficiency, uncertainty, temperature, and particle loss. This material is available free of charge via the Internet at <http://pubs.acs.org>.

### Literature Cited

- (1) Warwick, H.; Doig, A. *Smoke—The Killer in the Kitchen*; ITDG Publishing: London, 2004.
- (2) Bond, T. C.; Streets, D. G.; Yarber, K. F.; Nelson, S. M.; Woo, J.-H.; Klimont, Z. A technology-based global inventory of black and organic carbon emission from combustion. *J. Geophys. Res.* **2004**, *109* (D14), 203; <http://dx.doi.org/10.1029/2003JD003697>.
- (3) Intergovernmental Panel on Climate Change. *Climate Change 2001: The Scientific Basis*; Cambridge University Press: New York, 2001.
- (4) Rau, J. A. Composition and size distribution of residential wood smoke particles. *Aerosol Sci. Technol.* **1989**, *10*, 181–192.
- (5) Schauer, J. J.; Rogge, W. F.; Hildemann, L. M.; Mazurek, M. A.; Cass, G. R. Source apportionment of airborne particulate matter using organic compounds as tracers. *Atmos. Environ.* **1996**, *30* (22), 3837–3855.
- (6) Lim, H.-J.; Turpin, B. J.; Russell, L. M.; Bates, T. S. Organic and elemental carbon measurements during ACE-Asia suggest a longer atmospheric lifetime for elemental carbon. *Environ. Sci. Technol.* **2003**, *37* (14), 3055–3061.
- (7) Bucheli, T.; Gustafsson, Ö. Quantification of the soot–water distribution coefficient of PAHs provides mechanistic basis for enhanced sorption observations. *Environ. Sci. Technol.* **2000**, *34*, 5144–5151.
- (8) Oanh, N. T. K.; Reutergardh, L. B.; Dung, N. T. Emission of polycyclic aromatic hydrocarbons and particulate matter from domestic combustion of selected fuels. *Environ. Sci. Technol.* **1999**, *33*, 2703–2709.
- (9) Zhang, J.; Smith, K. R.; Ma, Y.; Ye, S.; Jiang, F.; Qi, W.; Liu, P.; Khalil, M. A. K.; Rasmussen, R. A.; Thorneloe, S. A. Greenhouse gases and other airborne pollutants from household stoves in China: A database for emission factors. *Atmos. Environ.* **2000**, *34*, 4537–4549.

- (10) Smith, K. R.; Khalil, M. A. K.; Rasmussen, R. A.; Thorneloe, S. A.; Manegdeg, F.; Apte, M. Greenhouse gases from biomass and fossil fuel stoves in developing countries: A manila pilot study. *Chemosphere* **1993**, *26*, 479–505.
- (11) Venkataraman, C.; Rao, G. U. M. Emission factors of carbon monoxide and size-resolved aerosols from biofuel combustion. *Environ. Sci. Technol.* **2001**, *35*, 2100–2107.
- (12) Bhattacharya, S. C.; Albina, D. O.; Abdul Salam, P. Emission factors of wood and charcoal-fired cookstoves. *Biomass Bioenergy* **2002**, *23*, 453–469.
- (13) Bertschi, I. T.; Yokelson, R. J.; Ward, D. E.; Christian, T. J.; Hao, W. M. Trace gas emissions from the production and use of domestic biofuels in Zambia measured by open-path Fourier transform infrared spectroscopy. *J. Geophys. Res.* **2003**, *108* (D13), 8469; <http://dx.doi.org/10.1029/2002JD002158>.
- (14) Ludwig, J.; Marufu, L. T.; Huber, B.; Andreae, M. O.; Helas, G. Domestic combustion of biomass fuels in developing countries: A major source of atmospheric pollutants. *J. Atmos. Chem.* **2003**, *44*, 23–37.
- (15) Brocard, D.; Lacaux, C.; Lacaux, J.-P.; Kouadio, G.; Yoboué, V. In *Biomass Burning and Global Change*; Levine, J. S., Ed.; MIT Press: Cambridge, MA, 1996.
- (16) Venkataraman, C.; Habib, G.; Eiguren-Fernandez, A.; Miguel, A. H.; Friedlander, S. K. Residential biofuels in South Asia: Carbonaceous aerosol emissions and climate impacts. *Science* **2005**, *307*, 1454–1456.
- (17) Martins, J. V.; Artaxo, P.; Lioussé, C.; Reid, J. S.; Hobbs, P. V.; Kaufman, Y. J. Effects of black carbon content, particle size, and mixing on light absorption by aerosols from biomass burning in Brazil. *J. Geophys. Res.* **1998**, *103* (D24), 32041–32050; <http://dx.doi.org/10.1029/98JD02593>.
- (18) Smith, K. R. *Biofuels, Air Pollution, and Health*; Plenum Press: New York, 1987.
- (19) Ezzati, M.; Lopez, A. D.; VanderHoorn, S.; Murray, C. J. L. Selected major risk factors and global and regional burden of disease. *Lancet* **2002**, *360*, 1347–1360.
- (20) Ballard-Tremere, G.; Jawurek, H. H. The “hood method” of measuring emissions of rural cooking devices. *Biomass Bioenergy* **1999**, *16*, 341–345.
- (21) United States Environmental Protection Agency. *Method 5H. Determination of Particulate Matter Emissions from Wood Heaters from a Stack Location*; U.S. Environmental Protection Agency: Washington, DC, 2000.
- (22) Abdol-Khalek, I.; Kittelson, D.; Brear, F. The influence of dilution conditions on diesel exhaust particle size distribution measurements. SAEI International Congress and Exposition, Detroit, MI: Society of Automotive Engineers: Warrendale, PA, 1999; Paper No. 1999-01-1142.
- (23) Lipsky, E. M.; Robinson, A. M. Effects of dilution on fine particle mass and partitioning of semivolatile organics in diesel exhaust and wood smoke. *Environ. Sci. Technol.* **2006**, *40*, 155–162.
- (24) Hildemann, L. M.; Cass, G. R.; Markowski, G. R. A dilution stack sampler for collection of organic aerosol emissions: Design, characterization and field-tests. *Aerosol Sci. Technol.* **1989**, *10* (1), 193–204.
- (25) Bond, T. C.; Anderson, T. L.; Campbell, D. Calibration and intercomparison of filter-based measurements of visible light absorption by aerosols. *Aerosol Sci. Technol.* **1999**, *30*, 582–600.
- (26) Arnott, W. P.; Moosmüller, H.; Sheridan, P. J.; Ogren, J. A.; Raspet, R.; Slaton, W. V.; Hand, J. L.; Kreidenweis, S. M.; Collett, J. L., Jr. Photoacoustic and filter-based ambient aerosol light absorption measurements: instrument comparisons and the role of relative humidity. *J. Geophys. Res.* **2003**, *108* (D1), 4034; <http://dx.doi.org/10.1029/2002JD002165>.
- (27) Wang, X.; Zhang, Y. Development of a critical airflow venturi for air sampling. *J. Agric. Eng. Res.* **1999**, *73*, 257–264.
- (28) Kirchstetter, T. W.; Corrigan, C. E.; Novakov, T. Laboratory and field investigation of the adsorption of gaseous organic compounds onto quartz filters. *Atmos. Environ.* **2001**, *35*, 1663–1671.
- (29) Gaur, S.; Reed, T. B. *Thermal Data for Natural and Synthetic Fuels*; Marcel Dekker: New York, 1998.
- (30) Haywood, J. M.; Shine, K. P. The effect of anthropogenic sulfate and soot aerosol on the clear sky planetary radiation budget. *Geophys. Res. Lett.* **1995**, *22*, 603–606.
- (31) Bohren, C. F.; Huffman, D. R. *Absorption and Scattering of Light by Small Particles*; Wiley-VCH Verlag GmbH & Co. KGaA: Weinheim, Germany, 2004.
- (32) Bond, T. C. Spectral dependence of visible light absorption by carbonaceous particles emitted from coal combustion. *Geophys. Res. Lett.* **2001**, *28*, 4075–4078.

- (33) Andreae, M.O.; Merlet, P. Emission of trace gases and aerosols from biomass burning. *Global Biogeochem. Cycles* **2001**, *15* (4), 955–966.
- (34) Kirchstetter, T. W.; Novakov, T.; Hobbs, P. V. Evidence that the spectral dependence of light absorption by aerosols is affected by organic carbon. *J. Geophys. Res.* **2004**, *109* (D21), 1208; <http://dx.doi.org/10.1029/2004JD004999>.
- (35) Pósfai, M.; Simonics, R.; Li, J.; Hobbs, P. V.; Buseck, P. R. Individual aerosol particles from biomass burning in southern Africa: 1. Compositions and size distributions of carbonaceous particles. *J. Geophys. Res.* **2003**, *108* (D13), 8483; <http://dx.doi.org/10.1029/2002JD002291>.
- (36) Kleeman, M. J.; Cass, G. R.; Eldering, A. Modeling the airborne particle complex as a source-oriented external mixture. *J. Geophys. Res.* **1997**, *102*, 21355–21372.
- (37) Turpin, B. J.; Lim, H.-J. Species contributions to PM<sub>2.5</sub> mass concentrations: revisiting common assumptions for estimating organic mass. *Aerosol Sci. Technol.* **2001**, *35*, 602–610.
- (38) Chow, J. C.; Watson, J. G.; Crow, D.; Lowenthal, D. H.; Merrifield, T. Comparison of IMPROVE and NIOSH carbon measurements. *Aerosol Sci. Technol.* **2001**, *34* (1), 23–34.
- (39) Novakov, T.; Corrigan, C. E. Thermal characterization of biomass smoke particles. *Microchim. Acta* **1995**, *119*, 157–166.
- (40) Dasch, J. M. Particulate and gaseous emissions from wood-burning fireplaces. *Environ. Sci. Technol.* **1982**, *16*, 639–645.
- (41) McDonald, J. D.; Zielinska, B.; Fujita, E. M.; Sagebiel, J. C.; Chow, J. C.; Watson, J. G. Fine particle and gaseous emission rates from residential wood combustion. *Environ. Sci. Technol.* **2000**, *34*, 2080–2091.
- (42) Malm, W. C.; Sisler, J. F.; Huffman, D.; Eldred, R. A.; Cahill, T. A. Spatial and seasonal trends in particle concentration and optical extinction in the United States. *J. Geophys. Res.* **1994**, *99*, 1347–1370.
- (43) Malm, W. C.; Day, D. E.; Kreidenweis, S. M.; Collett, J. L., Jr.; Carrico, C.; McMeeking, G.; Lee, T. Hygroscopic properties of an organic-laden aerosol. *Atmos. Env.* **2005**, *39*, 4969–4982.
- (44) Novakov, T.; Andreae, M. O.; Gabriel, R.; Kirchstetter, T. W.; Mayol-Bracero, O. L.; Ramanathan, V. Origin of carbonaceous aerosols over the tropical Indian Ocean: Biomass burning or fossil fuels? *Geophys. Res. Lett.* **2000**, *27* (24), 4061–4064.
- (45) Guazzotti, S. A.; Suess, D. T.; Coffee, K. R.; Quinn, P. K.; Bates, T. S.; Wisthaler, A.; Hansel, A.; Ball, W. P.; Dickerson, R. R.; Neusüss, C.; Crutzen, P. J.; Prather, K. A. Characterization of carbonaceous aerosols outflow from India and Arabia: Biomass/biofuel burning and fossil fuel combustion. *J. Geophys. Res.* **2003**, *108* (D15), 4485; <http://dx.doi.org/10.1029/2002JD003277>.

Received for review October 19, 2005. Revised manuscript received July 24, 2006. Accepted August 16, 2006.

ES052080I